
# Supplementary Materials for

## Crystallographic capture of a radical *S*-adenosylmethionine enzyme in the act of modifying tRNA

Erica L. Schwalm, Tyler L. Grove, Squire J. Booker, and Amie K. Boal.

correspondence to: squire@psu.edu or akb20@psu.edu

**This PDF file includes:**

## Materials and Methods

*Expression and Purification of RlmN C118A-tRNA$^{Glu}$ in vivo cross-link and free RlmN C118A.*

The RlmN C118A variant was expressed as previously described except IPTG was added to a final concentration of 250 μM prior to induction (*20*). All purification steps were performed in an anaerobic chamber (Coy Laboratory Products). In a typical purification, 30 grams of cell paste were resuspended in 150 mL of lysis buffer [50 mM HEPES, pH 7.5, 300 mM potassium chloride, 4 mM imidazole, 10 mM 2-mercaptoethanol (BME), 10 mM magnesium chloride, and 10% glycerol] containing 0.1% Triton-X100. Lysozyme and DNase I were added (final concentrations of 1 mg/mL and 0.1 mg/mL, respectively) and, after stirring at room temperature for 30 minutes, the lysate was placed in an ice bath and cooled to 4 °C. The solution was subjected to 6 rounds of sonic disruption (30% output, 45 s pulse time) with intermittent pausing for 8 minutes to maintain a temperature of 4 °C. The lysate was cleared via centrifugation at 4°C for 1 hour at 40,000 × *g*. The supernatant was loaded onto a $Co^{2+}$-Talon resin column equilibrated in lysis buffer lacking Triton-X100. The column was washed with 200 mL of lysis buffer before elution with 100 mL of elution buffer (50 mM HEPES, pH 7.5, 300 mM potassium chloride, 300 mM imidazole, 10 mM magnesium chloride, 10 mM BME, and 10% glycerol). Fractions containing significant brown color were pooled and concentrated to 2 mL using a Centricon-10 ultrafiltration device. The solution was desalted using a PD-10 column equilibrated in Buffer A (50 mM Tris-HCl, pH 8.0, 50 mM NaCl, 5 mM DTT) containing 10% glycerol and diluted to a final volume of 3 mL. To remove the portion of protein that forms a covalent cross-link during heterologous overexpression (*in vivo* cross-linked C118A RlmN), the isolated protein was further purified by anion-exchange chromatography. At this point, the protein was loaded onto a HiPrep QFF 16/10 column (20 mL) interfaced with an ÄKTA FPLC and either **Method 1** or **Method 2** was applied to the column to purify free RlmN C118A or RlmN C118A-tRNA$^{Glu}$ *in vivo* cross-link, respectively. **Method 1**: The HiPrep QFF 16/10 column was equilibrated in Buffer A. The protein was loaded onto the column and washed with one column volume (CV) of Buffer A. Then, a linear gradient up to 70% Buffer B (50 mM Tris-HCl, pH 8.0, 1 M NaCl, 5 mM DTT) was applied over 12 CV to separate free protein from the *in vivo* cross-linked C118A RlmN. The fractions corresponding to free protein were pooled and concentrated to 2 mL as described above. The final protein was desalted using a PD-10 column equilibrated in 20 mM HEPES, pH 7.5, 500 mM potassium chloride, 5 mM magnesium chloride, 5 mM DTT and 10% glycerol, and stored under liquid nitrogen. Protein concentration was determined using a calibrated Bradford assay (*20*). **Method 2**: The HiPrep QFF 16/10 column was equilibrated in Buffer A. The protein was loaded onto the column and washed with 2.5 CV of Buffer A. Then, a linear gradient from 0 % to 12 % Buffer B (50 mM Tris-HCl, pH 8.0, 2 M NaCl, 5 mM DTT) was applied over 1 CV. Free RlmN C118A elutes at the end of this gradient. The percentage of Buffer B was increased from 12% to 25% over 10.5 CV. The RlmN C118A *in vivo* cross-linked species elutes between 20-25% Buffer B (Figure S2A). The concentration of Buffer B was increased to 100% over 3 CV and then maintained at this concentration for 2 CV to remove any remaining material and to recharge the resin. Fractions corresponding to the cross-linked species were pooled and concentrated to

~200 µL (~ 50 mg•mL$^{-1}$). The final protein was mixed with 50 µL of 50% glycerol, flash frozen and stored under liquid nitrogen. Protein concentration was determined using a Bradford assay with the correction factor of 0.76 (*20*).

*Synthesis and purification of tRNA$^{Glu}$.*

The DNA template for *in vitro* transcription of tRNA$^{Glu}$ was produced by overlap primer extension using the following primers, in which the bold portion indicates the T7 RNA polymerase promoter and the underlined portion represents the overlapping sequence: tRNA$^{Glu}$ For (5'-gggaaatt**aatacgactcactatag**tccccttcgtctagaggccccggacaccgccc-3') and tRNA$^{Glu}$ Rev (5'-tmggcgtcccctaggggattcgaacccctgttaccgccgtgaaagggcggtgtcc-3'). Full-length tRNA was produced by *in vitro* transcription with His$_6$-tagged T7 RNA polymerase. A typical transcription reaction contained 30 mM Tris-HCl, pH 8.4, 20 mM DTT, 26 mM $MgCl_2$, 0.01% Triton X-100, 2 mM spermidine, 4 mM of each NTP, 5 ng/µL DNA template, and 4 mg of T7 RNA polymerase in a final volume of 10 mL. The transcription reaction was mixed and incubated at 37° C for 1.5 hours. 100 U of DNase I (RNAse free, New England BioLabs) was added and incubated for an additional hour at 37° C. The reaction was quenched with the addition of 50 mM EDTA and precipitate was removed by centrifugation. The liquid portion of the reaction was transferred to a new conical tube, and the RNA was recovered by ethanol precipitation with three volumes of cold ethanol after the addition of 300 mM sodium acetate. The mixture was stored at -20° C until further purification. Precipitated RNA was collected by centrifugation and the pellet was resuspended in sterile water, followed by desalting via a PD-10 column equilibrated in sterile water. The RNA was collected and diluted to a concentration of less than 100 µM. Dilute RNA was heated above the melting temperature for five minutes and slowly cooled to room temperature. The refolded RNA was concentrated using a Centricon 10 (MWCO 10 kDa) centrifugal filter device. The final concentration was determined from an extinction coefficient (0.890 µM$^{-1}$ cm$^{-1}$ at 260 nm) calculated using OligoCalc (*37*).

*Preparation and purification of the RlmN C118A-tRNA$^{Glu}$ in vitro cross-linked intermediate.*

RlmN C118A was overexpressed and purified as described above. A typical reaction contained 100 mM EPPS, pH 8.0, 20 mM $MgCl_2$, 2 mM SAM, 50 µM flavodoxin, 25 µM flavodoxin reductase, 125 µM purified RlmN C118A, and 150 µM tRNA$^{Glu}$ in a total volume of 1.5 mL. The mixture was incubated for 3 minutes at room temperature before the addition of 2 mM NADPH to initiate the reaction. The reaction was allowed to proceed for 1 hour prior to purification. The reaction mixture was desalted using a PD-10 column equilibrated in Buffer A (50 mM TRIS-HCl, pH 8.0, 50 mM NaCl, 5 mM DTT) containing 10% glycerol, and diluted to a final volume of 3 mL. The mixture was loaded onto a HiPrep QFF 16/10 column equilibrated in Buffer A, and the column was washed with one CV of the same buffer. A linear gradient from 0 to 70% Buffer B (50 mM Tris-HCl, pH 8.0, 1 M NaCl, 5 mM DTT) was applied over 12 CV to separate the cross-link from unreacted components (Figure S2B). The concentration of Buffer B was increased to 100% over 1 CV and then kept at this concentration for 2 CV to remove any remaining material. The peak corresponding to cross-linked RlmN was collected and concentrated using a Centricon 10 (MWCO 10 kDa) centrifugal filter

device. The presence of the cross-link was confirmed by observation of a high MW band during SDS-PAGE analysis (*25*), and the concentration of the protein component was determined by Bradford assay.

*Crystallization of the RlmN C118A-tRNA$^{Glu}$ in vivo and in vitro cross-linked intermediates.*

All manipulations were performed in a Coy anaerobic chamber. The cross-linked protein solutions prepared *in vivo* or *in vitro*, containing 2 mM $MgCl_2$ and 8-10 mg/mL cross-linked C118A RlmN (based on protein concentration), were diluted from concentrated stocks (≥ 50 mg/mL) with water. The solutions were passed through a 2.0 μm spin filter prior to crystallization trial setup. For the *in vivo* cross-linked species, brown rectangular rod-shaped crystals were obtained within one week using the hanging drop vapor diffusion method at room temperature with 10% (w/v) PEG 4000, 0.2 M potassium chloride, 0.05M magnesium chloride, and 0.05 M Tris-HCl, pH 7.5, as the precipitating reagent equilibrated against a 0.5 M LiCl well solution. Crystals were briefly dipped in cryoprotectant (25% (v/v) glycerol, 10% (w/v) PEG 4000, 0.2 M potassium chloride, 0.05M magnesium chloride, and 0.05 M Tris-HCl, pH 7.5), mounted on rayon loops, and flash frozen in liquid nitrogen. For the *in vitro* cross-link, crystals were obtained using the hanging drop vapor diffusion method at room temperature with 10% (w/v) PEG 4000, 0.1 M sodium chloride, 0.05 M sodium cacodylate trihydrate, pH 6.0, and 0.5 mM spermine as the precipitating reagent equilibrated against a 0.5 M LiCl well solution. The crystals were briefly dipped in cryoprotectant (30% (v/v) glycerol, 10% (w/v) PEG 4000, 0.1 M sodium chloride, 0.05 M sodium cacodylate trihydrate, pH 6.0, 0.5 mM spermine), mounted on rayon loops, and flash frozen in liquid nitrogen.

*Structure solution of the RlmN C118A-tRNA$^{Glu}$ in vivo cross-linked intermediate.*

X-ray diffraction datasets were collected at the General Medical Sciences and Cancer Institutes Collaborative Access Team (GM/CA-CAT) beamlines at the Advanced Photon Source and processed using the HKL2000 package (*38*). The structure was solved by molecular replacement using Phaser-MR in the Phenix software package (*39*) with chain B from the RlmN+SAM structure (PDB accession code 3RFA) as the search model. All cofactors (SAM and the [4Fe–4S] cluster) and water molecules associated with the search model were omitted prior to molecular replacement. Manual model building and refinement were performed using Coot, phenix.refine, and Refmac5 (*40-42*). The initial search located two molecules of RlmN in the asymmetric unit. Residues 351-374 displayed evidence of conformational change in the initial maps and were manually remodeled to fit the new electron density. After modeling the [4Fe–4S] clusters, strong $F_o$-$F_c$ electron density was observed between the side chain of mCys355 and unmodeled electron density associated with the tRNA substrate. The RCrane extension (ver. 1.1) (*43*) in Coot was used to model an adenosine adjacent to Cys355, and cytosine nucleotides were built into additional electron density in the 5' and 3' direction along the strand. Modeling and refinement of approximately 50 nucleotides in this fashion allowed for assignment of the RNA molecule as a tRNA. RlmN modifies six different tRNA molecules, four of which have a guanosine adjacent to the target A37. The quality of the electron density map corresponding to the nucleotides 5' and 3' to A37 allowed for differentiation between guanosine and cytosine bases. The tRNA molecule could only be

assigned as $tRNA^{Asp}_{GUC}$ or $tRNA^{Glu}_{UUC}$ because these are the only RlmN targets that have cytosines flanking A37 at the 5'-end, excluding the other four tRNA substrates that have adjacent guanosines. To differentiate between $tRNA^{Asp}_{GUC}$ and $tRNA^{Glu}_{UUC}$, models of each of the candidate tRNAs were generated with the correct sequences for the 50 nucleotides surrounding A37. Manual building and refinement of the models allowed $tRNA^{Glu}_{UUC}$ to be unambiguously assigned as the *in vivo* cross-linked species based on visual inspection of the electron density map and improvement in the $R_{work}$ and $R_{free}$ statistics. Further refinement and model building were performed using the $tRNA^{Glu}_{UUC}$ sequence. In the later stages of refinement, TLS groups were assigned (*41*) and used in subsequent rounds. JLigand (*44*) was used to generate the refinement parameters for the Cys355-A37 covalent cross-link, including $sp^3$ hybridization at C2 in A37. The final model consists of residues 18 to 371 for both chains A and B, nucleotides 2 to 69 for chain C and D, 8 iron ions, 8 sulfide ions, 2 molecules of 5'-deoxyadenosine, 2 molecules of methionine, 6 magnesium ions, and 66 water molecules. Data collection and refinement statistics are shown in Table S1.

*Structure solution of the RlmN C118A-$tRNA^{Glu}$ in vitro cross-linked intermediate.*

X-ray diffraction datasets were collected at the Life Sciences Collaborative Access Team (LS-CAT) beamlines at the Advanced Photon Source and processed using the HKL2000 package (*38*). The structure was solved by molecular replacement using Phaser (*39*) and previously published RlmN (3RFA) and $tRNA^{Glu}$ structures (PDB accession code 2DER) as separate components of the search model. Nucleotides 32-39 were deleted from the starting coordinates of $tRNA^{Glu}$ as this region showed significant perturbations in initial electron density maps. Manual model building and refinement were performed using Coot and Refmac5, respectively (*40, 42*). The final model consists of residues 16 to 375 for chain A and B, nucleotides 3 to 71 for chain C and D, 8 iron atoms, 8 sulfur atoms, 2 molecules of 5'-deoxyadenosine, 2 molecules of methionine, 7 magnesium ions, and 123 water molecules.

*Activity determination of RlmN using in vitro transcribed tRNA and 155-mer RNA substrates.*

The ability of RlmN to catalyze methylation reactions on the unmodified tRNA substrates was tested for all six tRNAs suggested to be modified by RlmN. Each reaction contained 5 μM RlmN Wt, 100 μM tRNA, 100 mM EPPS, pH 8.0, 20 mM $MgCl_2$, 2 mM SAM, and 2 mM dithionite in a final volume of 100 μL. Reactions were allowed to proceed for one hour before a 20 μL aliquot was quenched with 20 μL of 50 mM sulfuric acid containing 100 μM tryptophan as an internal standard. 40 μL of 250 mM sodium acetate, pH 6.0, 45 mM NaCl, and 4 mM $ZnCl_2$ was added to each quenched reaction before the addition of 5 U of Antarctic phosphatase and 0.5 U of P1 nuclease. The solutions were incubated at 37° C overnight to allow for complete digestion of the tRNA. The production of 2-methyladenosine ($m^2A$) was quantified using LC-MS as previously described (*21*). The rate of methylation of unmodified $tRNA^{Glu}$ by RlmN was tested and compared to activity using the 155-mer 23S rRNA substrate established previously to be an effective substrate for wt RlmN (*21*). The 155-mer was prepared as described previously except sterile water was used for purification in place of the buffer described (*21*). Reaction mixtures contained the following in a final volume of 100 μL: 100 mM

EPPS, pH 8.0, 20 mM $MgCl_2$, 2 mM SAM, 100 μM RNA substrate, 50 μM flavodoxin, 25 μM flavodoxin reductase, 2 mM NADPH, and 5 μM wt RlmN. Reactions were initiated by the addition of NADPH after incubation of all other components for 3 minutes. 10 μL aliquots were taken from the reaction mixture at specified times and quenched in 10 μL of 50 mM $H_2SO_4$ containing 100 μM L-tryptophan as an internal standard. After collection of all time points, 20 μL of 250 mM sodium acetate, pH 6.0, 45 mM NaCl, and 4 mM $ZnCl_2$ was added to each quenched aliquot to allow for RNA digestion. The solution was mixed prior to the addition of 0.5 U of P1 nuclease and 5 U of Antarctic phosphatase. The solutions were mixed again and incubated at 37° C overnight to allow for complete digestion of the RNA substrates. The concentrations of products were determined by LC-MS analysis as previously described (*20*).

*Construction, overexpression, and purification of RlmN R206A.*

An arginine to alanine substitution at R206 was generated using the Stratagene Quikchange II kit (Agilent Technologies) and the following primers, in which the altered codons are shown in boldface: RlmN R206A For (5'-ggt ttt ggc ctg tct aaa **GCG** cgc gtc acg ctt tcc act tcc-3') and RlmN R206A Rev (5'-gga agt gga aag cgt gac gcg **CGC** ttt aga cag gcc aaa acc-3'). Vent DNA polymerase was used in place of the *Pfu* polymerase recommended in the kit protocol. Protein containing the arginine to alanine substitution (RlmN R206A) was overexpressed and purified as described for wt RlmN (*20*).

*Activity Determination of RlmN R206A.*

Enzymatic assay of RlmN R206A using $tRNA^{Glu}$ and 155-mer as substrates was performed as described above.

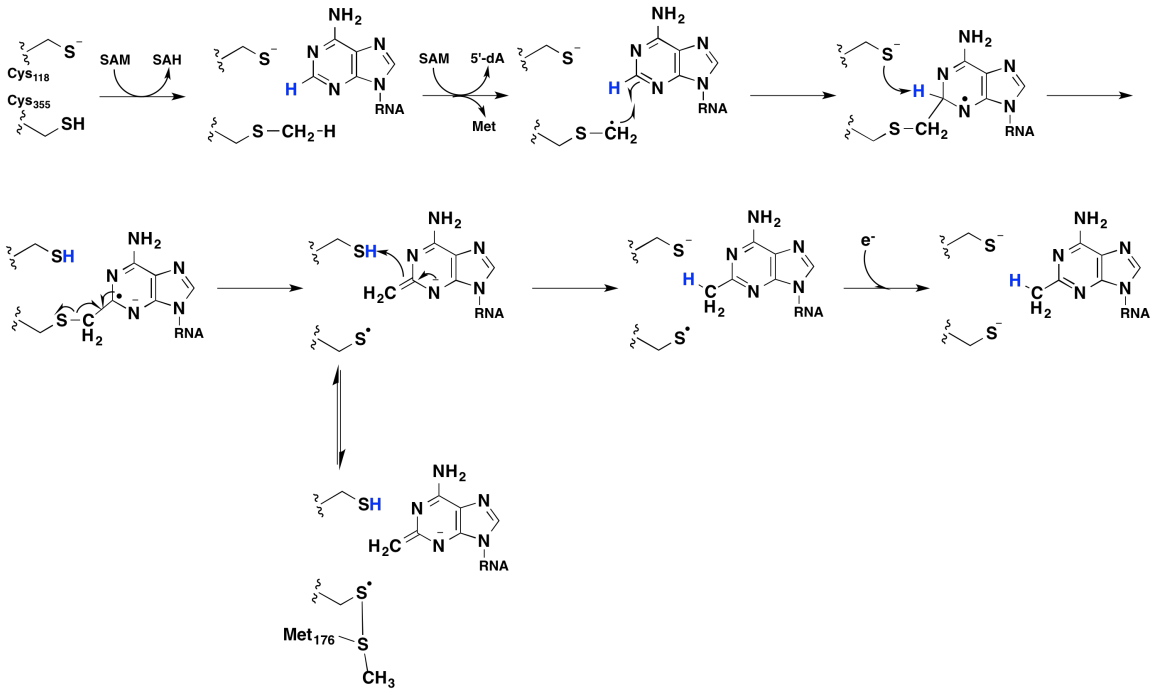


**Fig. S1.**

Proposed mechanism for RlmN-catalyzed methylation of ribosomal or transfer RNA at the C2 position of a substrate adenosine base.

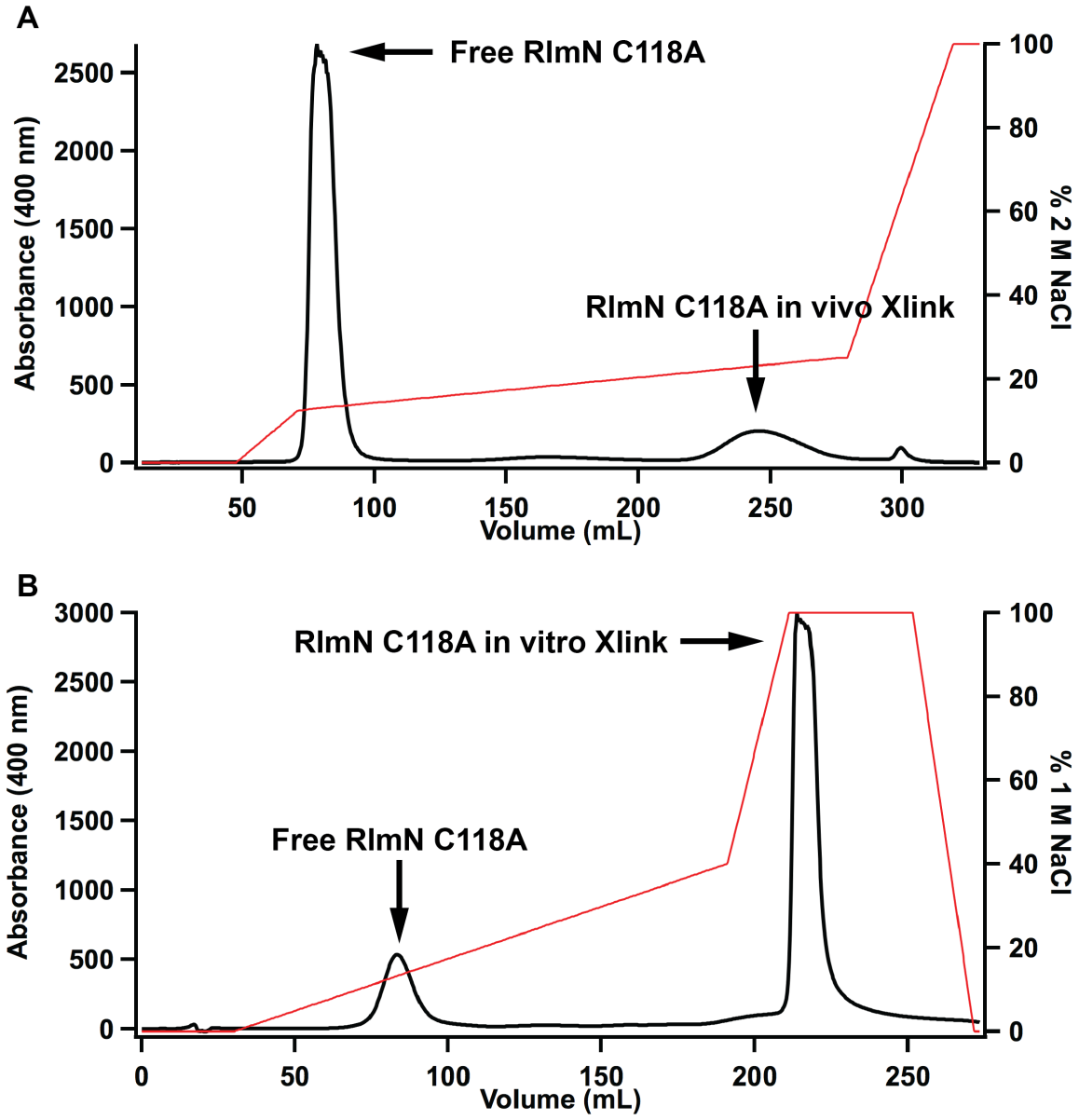


**Fig. S2**

Anion-exchange chromatograms of the RlmN C118A *in vivo* (**A**) and *in vitro* cross-link (**B**) samples.

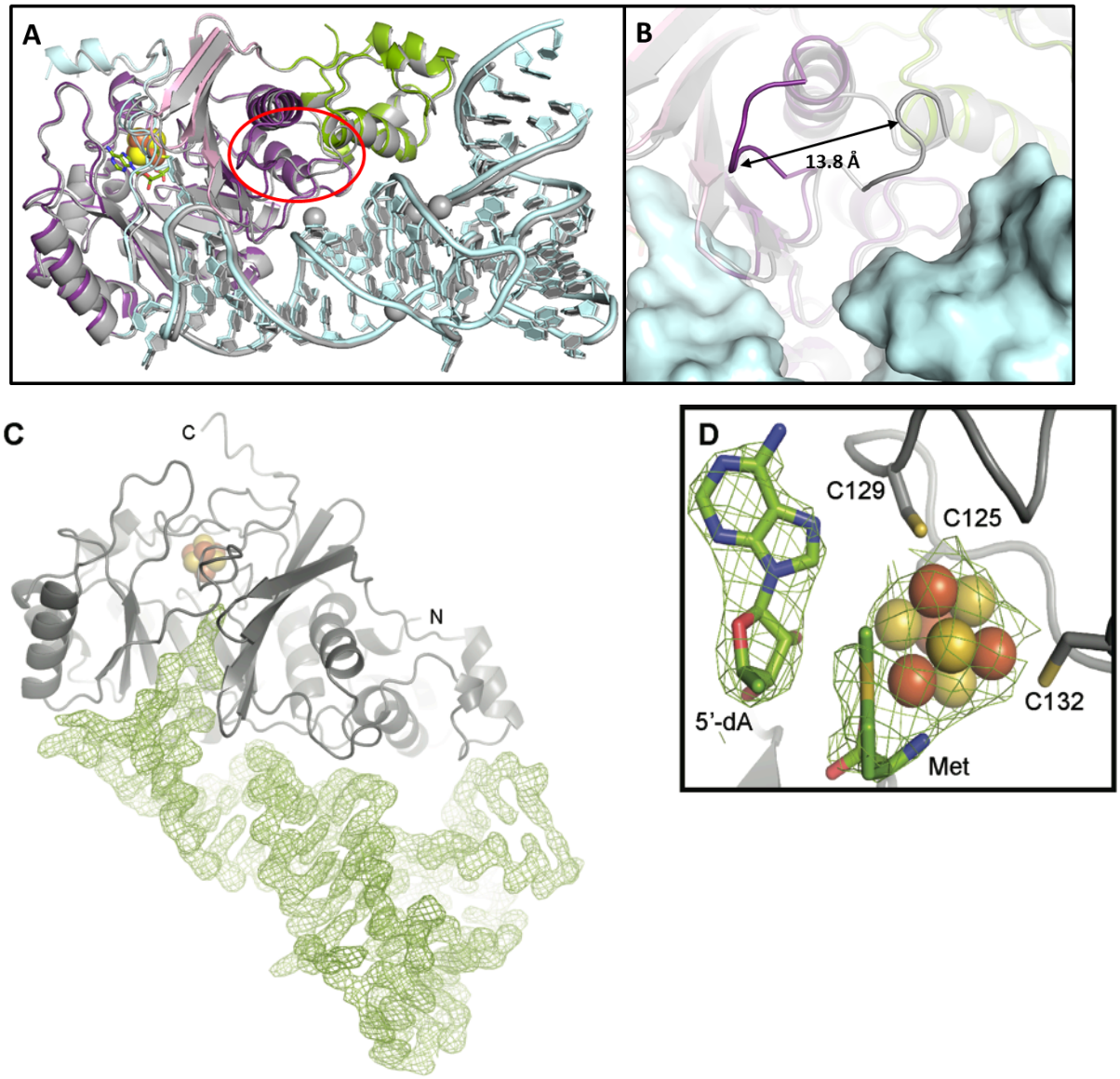


**Fig. S3**

Overlay of the *in vivo* and *in vitro* RlmN tRNA$^{Glu}$ cross-link structures. (**A**) Pairwise secondary structure matching structural alignment between RlmN tRNA$^{Glu}$ crosslinked structures generated *in vivo* (gray) or *in vitro* (colored) (rmsd 1.0 Å over 692 residues). The only significant structural difference is observed in the loop connecting a1/b2 (residues 163-168, red circle). (**B**) Zoomed-in view of the loop. Residues 163-168 shift by 13.8 Å towards the phosphate backbone of the tRNA substrate (shown as a teal surface) in the *in vivo* cross-link structure (highlighted in red). The shift allows the loop to make non-specific van der Waals contacts with the RNA molecule. The region adopts different conformations in previously published structures of RlmN suggesting high flexibility and a propensity to shift between these conformations based on subtle differences in crystal packing. (**C**) Omit map (green mesh, 1.5s) showing electron density for the nucleic acid component in the in vivo crosslinked structure. (**D**) Omit map (green mesh, 1.5s) for the 5'-dA and methionine (Met) byproducts trapped in the active site.

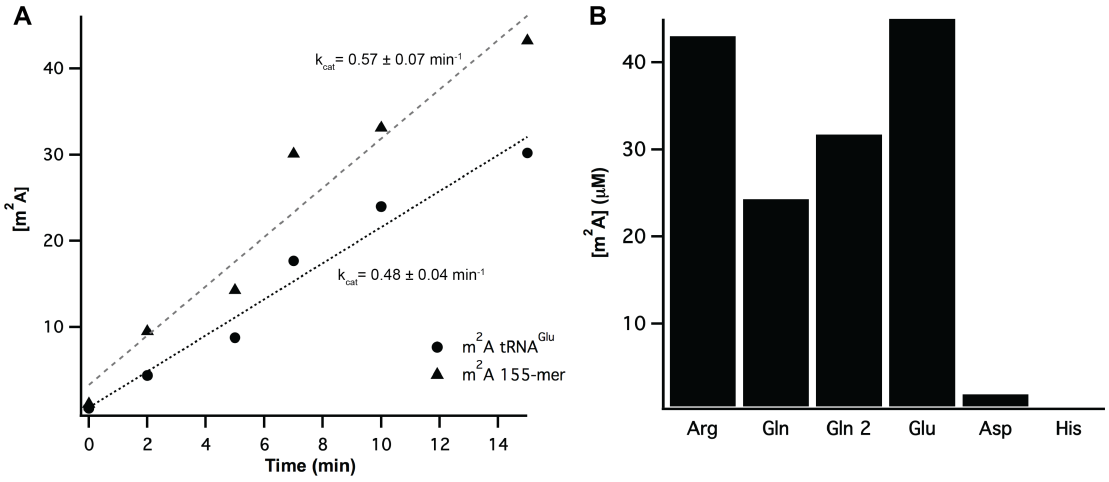


**Fig. S4**

Activity assays for wt RlmN with 155-mer rRNA and $tRNA^{Glu}$ substrates. (**A**) The rate of production of 2-methyladenosine by wt RlmN is shown for reactions using 155-mer rRNA (triangles) and $tRNA^{Glu}$ (circles). Each reaction was performed for 15 minutes at room temperature with 100 mM EPPS, pH 8.0, 20 mM $MgCl_2$, 2 mM SAM, 50 uM flavodoxin, 25 uM flavodoxin reductase, 5 uM RlmN, and 100 uM RNA substrate. Fit of the data to a straight line yields $k_{cat}$ of 0.57 min$^{-1}$ and 0.48 min$^{-1}$ for the 155-mer and $tRNA^{Glu}$, respectively. Thus we conclude that *in vitro* transcribed tRNA is a viable substrate for the RlmN reaction as it supports similar turnover when compared to the 155-mer rRNA transcript, previously shown to be an effective substrate for RlmN. (**B**) Production of 2-methyladenosine by wt RlmN using the tRNA substrates proposed based on knowledge of C2 modification *in vivo*. Each reaction contained 5 μM RlmN, 100 μM tRNA, 100 mM EPPS pH 8.0, 20 mM $MgCl_2$, 2 mM SAM, and 2 mM dithionite. Reactions were allowed to proceed for one hour at room temperature. $tRNA^{Arg}$ and $tRNA^{Glu}$ show the greatest production of $m^2A$, while $tRNA^{His}$ and $tRNA^{Asp}$ do not accumulate significant product.

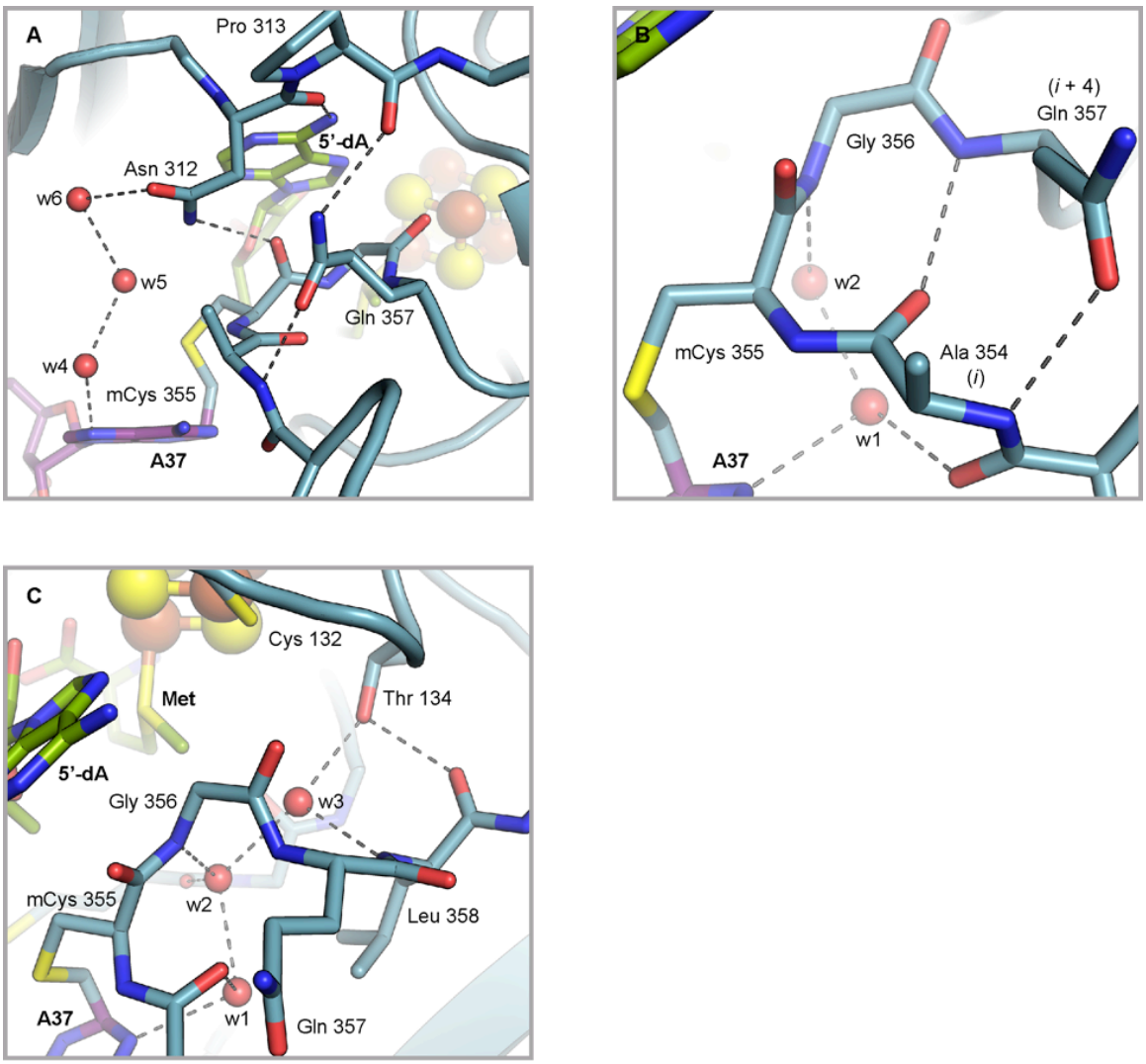


**Fig. S5**

Three additional views of the secondary structure and extended hydrogen bonding network associated with the C-terminal extension loop containing mCys 355. The sequence pattern in the loop is reminiscent of similar conserved loop sequences found in glycyl radical enzymes (*45*), with potential structural and mechanistic connections to RlmN (*26*). Most significantly, the small Ala/Gly side chains flanking the H• abstraction target in RlmN allow mCys 355 to make a close approach to the site of 5'-dA• formation (**A**), necessary for H-atom abstraction, and provide the requisite backbone conformational flexibility to ensure that the correct contacts can be made to the A37 base. Gln 357 further stabilizes the b-turn motif (**B**) via a hydrogen bond to the backbone amide nitrogen of Ala 354. Leu 358 packs against ordered water molecules (w1, w2) that mediate interaction between the loop and the substrate adenine. Extension of this network to include RlmN structural motifs that define the iron-sulfur cluster (**C**) and the 5'-dA/SAM binding sites (**A**) further ensure stabilization of the loop in a conformation critical for initiation of catalysis.

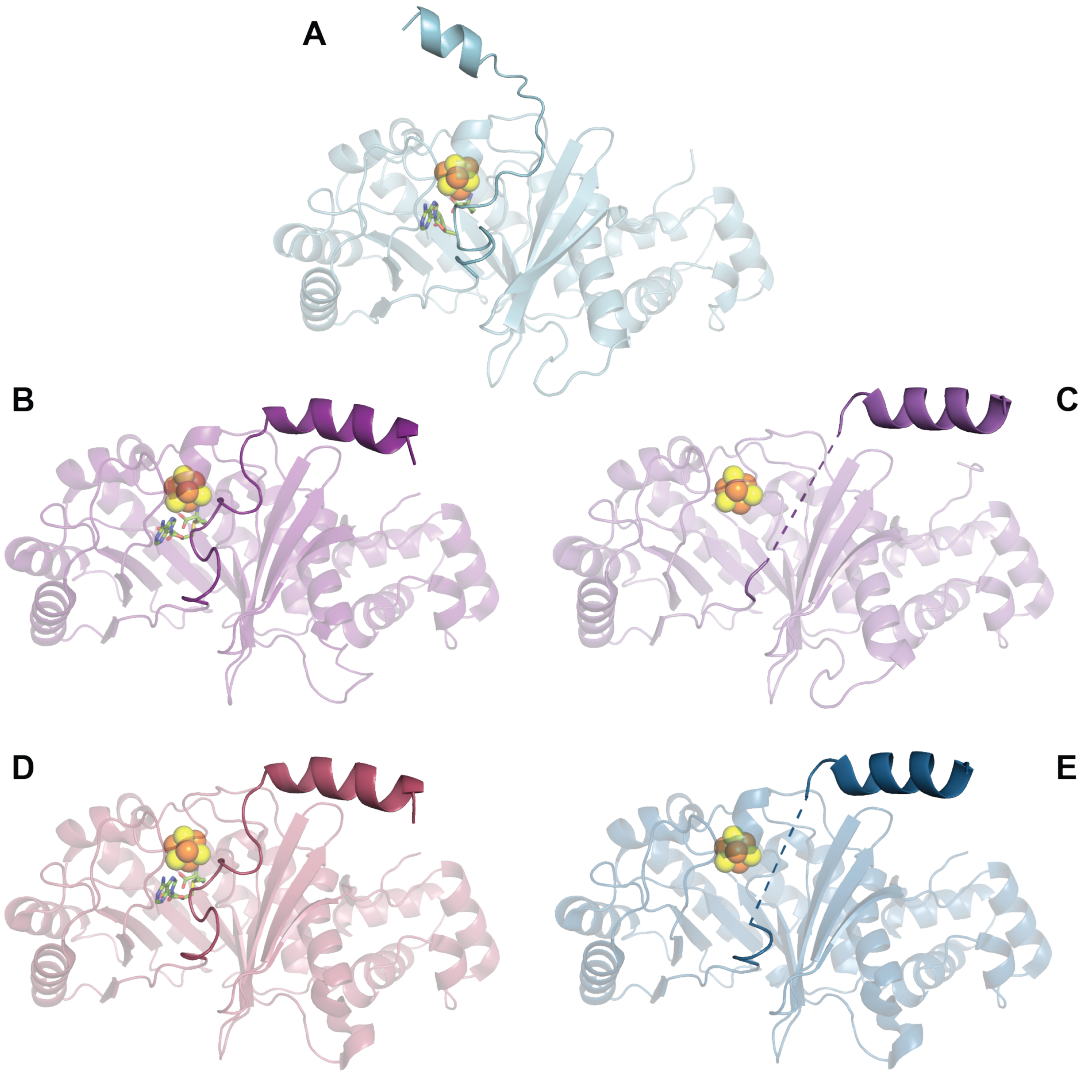


**Fig. S6**

Comparison of the five structures of RlmN reported to date. RlmN is shown in cartoon format in all structures shown. These include the *in vitro* tRNA cross-link structure reported here (A), wt RlmN with SAM (PDB accession code 3RFA) (B), wt RlmN without SAM (PDB accession code 3RF9) (C), RlmN C118A with SAM (PDB accession code 4PL1) (D), and RlmN C118A without SAM (PDB accession code 4PL2) (E). The [4Fe-4S] is shown as a space-filling model, with SAM, 5'-dA, and methionine shown as sticks when present. Disordered regions are represented with dashed lines. The overall protein architecture changes little in all 5 structures. The C-terminal extension, however, exhibits significant conformational change in response to binding of SAM or RNA and is darkened for emphasis. The Cys355 loop is disordered in the absence of SAM and resides in two distinct locations in the presence and absence of the RNA substrate. The flexibility of this loop likely facilitates the complex reaction that occurs at the active site.

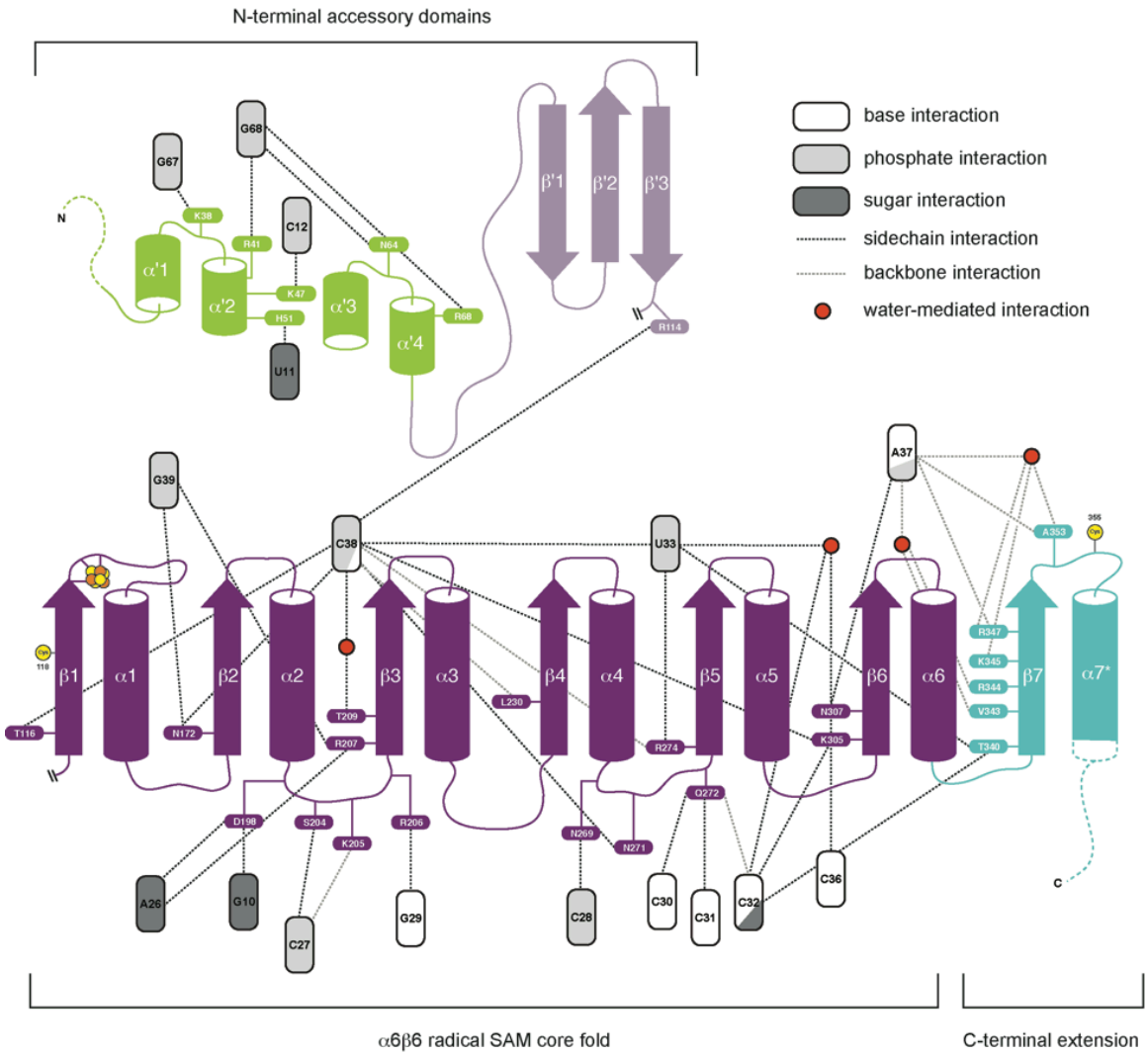


**Fig. S7**

RlmN topology diagram illustrating protein-nucleic acid interactions, predominantly localized to the accessory domains and extensions or connecting loop segments between secondary structure elements in the core fold. A modular strategy for substrate interaction is consistent with observation of extra domains and structural elements in other radical SAM enzymes that target large macromolecular substrates.

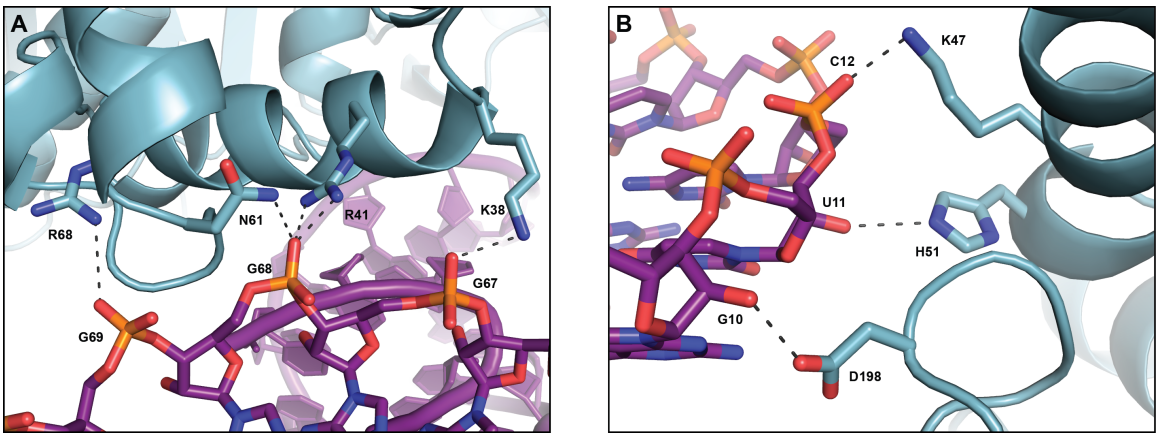


**Fig. S8**

Detailed views of the hydrogen bonding interactions between RlmN and $tRNA^{Glu}$ located outside the anti-codon stem loop. (A) View of the interactions found in the N-terminal domain of RlmN. Residues 38, 41, 61, and 68 are shown as sticks and colored by atom type. Dashed lines represent hydrogen bonding interactions between RlmN and the 3'-end of $tRNA^{Glu.}$. All bonds in this region occur between protein side chains and backbone phosphates. The lack of base-specific interactions suggests that the N-terminal domain of RlmN recognizes overall RNA structure rather than a specific sequence, although its mode of recognition may be different with ribosomal RNA. (B) Views of the hydrogen bonding interactions between RlmN and $tRNA^{Glu}$ in the mid-region of the tRNA. K47, H51, and D198 are shown as sticks and colored by atom type. Dashed lines represent hydrogen bonding interactions between the protein side chains and tRNA. D198 and H51 interact with the 2'-hydroxyl of the specified bases while K47 contacts the phosphate backbone. This region also lacks base-specific interactions, supporting shape recognition of tRNA by these motifs as well.

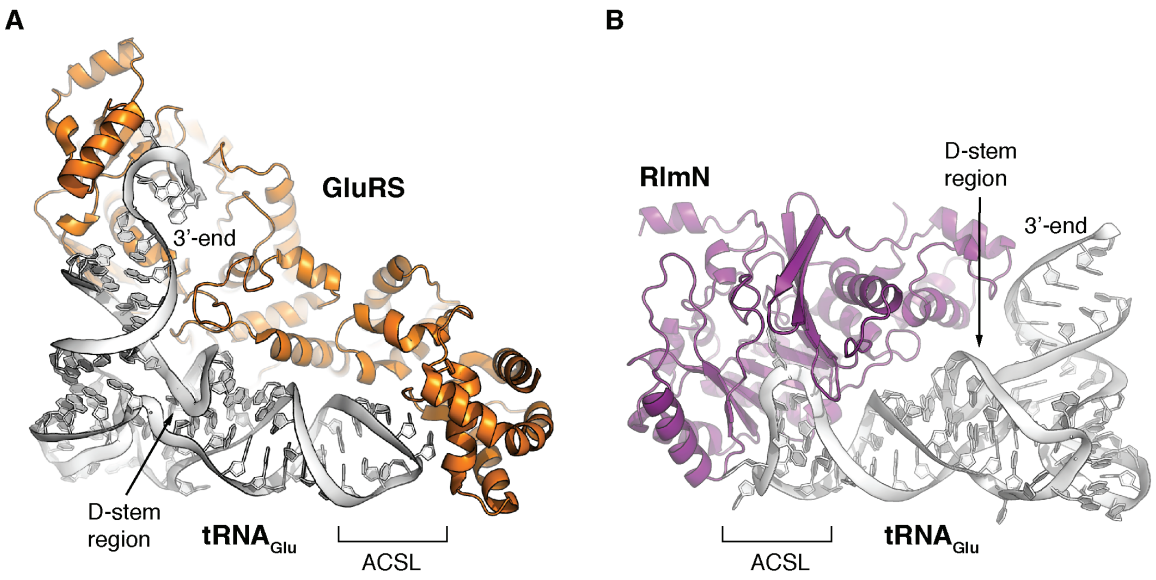


**Fig. S9**

Comparison of the *Thermus thermophilus* $tRNA_{Glu}$ in complex with GluRS tRNA synthetase (PDB accession code 2CV0) (A) and *E. coli* RlmN bound to $tRNA_{Glu}$ (B). The two systems interact with the entire tRNA molecule in three key regions at the anticodon stem loop (ACSL), in the D-stem region, and at the 3'-end.

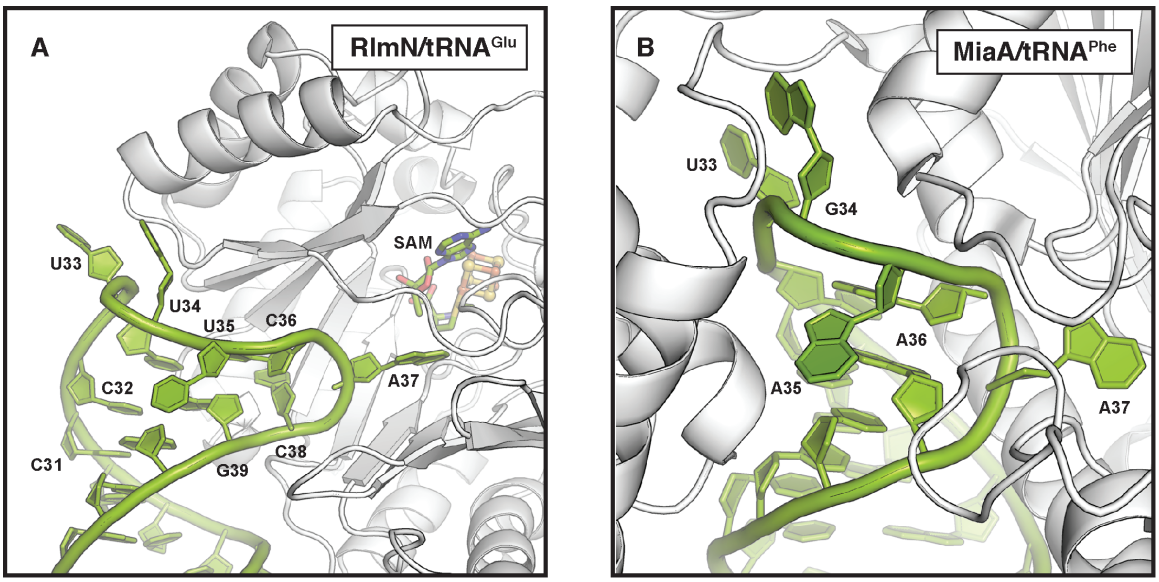


**Fig. S10**

Comparison of the β7-induced ACSL distortion observed in RlmN/tRNA$^{Glu}$ complex (A) with a similar distortion found in MiaA, another tRNA modification complex that targets the same position. MiaA (PDB accession code 2ZM5) employs an α-helix to initiate base-flipping of A37 in tRNA$^{Phe}$.

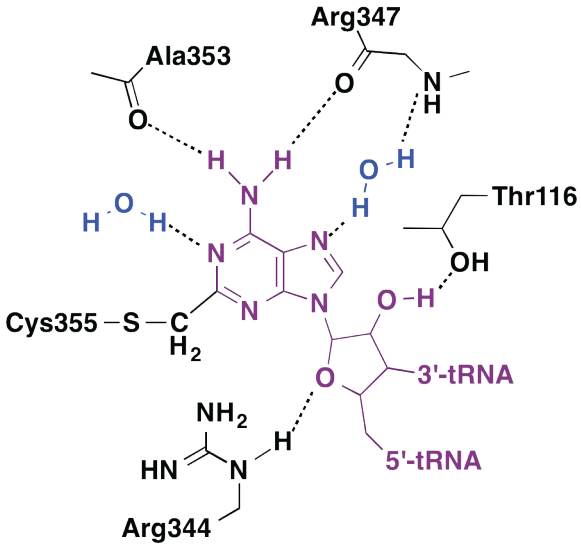


**Fig. S11**

A diagram of the binding pocket of adenosine-37 of $tRNA^{Glu}$. A37 makes significant hydrogen bonding interactions with the protein, positioning the nucleotide for methylation. The RNA is shown in purple, protein in black, and coordinated water molecules in blue. Backbone carbonyls of Ala353 and Arg347 form hydrogen bonds with the exocyclic amine of A37. A water-mediated hydrogen bond is formed between N7 of A37 and the backbone nitrogen of Arg347. The Thr116 side chain H-bonds to the 2'-hydroxyl of the ribose ring while Arg344 coordinates O3. These two interactions hold the sugar in place and facilitate binding of the adenine in the pocket.

**Table S1.**

Crystallographic data collection and refinement statistics

| | RlmN *in vitro* Xlink[1] | RlmN *in vivo* Xlink[2] |
|---|---|---|
| **Data collection** | | |
| Wavelength (Å) | 0.9786 | 1.0332 |
| Space group | $P2_1$ | $P2_1$ |
| Cell dimensions | | |
| *a*, *b*, *c* (Å) | 90.72, 70.38, 151.81 | 88.66, 69.82, 149.30 |
| α, β, γ (°) | 90.00, 90.11, 90.00 | 90.00, 90.30, 90.00 |
| Resolution (Å) | 50.00-2.40 (2.44-2.40) | 50.0-2.88 (2.98 - 2.88) |
| $R_{sym}$ or $R_{merge}$ | 0.087 (0.529) | 0.117 (0.867) |
| $R_{pim}$ | 0.026 (0.362) | 0.059 (0.500) |
| $CC_{1/2}$ | 0.800 | 0.754 |
| $\langle I/\sigma I \rangle$ | 34.9 (1.8) | 19.1 (3.1) |
| Reflections | | |
| Measured | 547663 | 147646 |
| Unique | 75380 | 23364 |
| Completeness (%) | 99.9 (99.2) | 99.0 (94.3) |
| Redundancy | 7.3 (5.7) | 6.3 (6.8) |
| Wilson B Factor (Å$^2$) | 59.7 | 71.2 |
| | | |
| **Refinement** | | |
| Resolution (Å) | 50.0-2.40 | 50.0-2.88 |
| No. reflections | 71560 | 43895 |
| $R_{work}$ / $R_{free}$ | 0.216/0.248 | 0.187/0.237 |
| No. atoms | 8837 | 8482 |
| Protein | 5694 | 8405 |
| RNA | 2972 | |
| Ligand/ion | 77 | 56 |
| Water | 94 | 21 |
| *B*-factors (Å$^2$) | | |
| Protein | 61 | 66. |
| RNA | 71 | |
| Ligand/ion | 54 | 53 |
| Water | 54 | 49 |
| R.m.s. deviations | | |
| Bond lengths (Å) | 0.005 | 0.060 |
| Bond angles (°) | 1.01 | 1.00 |
| Ramachandran Statistics (%) | | |
| Favored | 97.4 | 93.2 |
| Outliers | 0.0 | 0.4 |

[1]Data collected at LS-CAT beamline 21-ID-G

[2]Data collected at GM/CA-CAT beamline 23-ID-B